PHOSPHOPROTEOMICS

Targeted phosphoproteomics of insulin signaling using data-independent acquisition mass spectrometry

Benjamin L. Parker,[1,2]* Guang Yang,[1,2]* Sean J. Humphrey,[3] Rima Chaudhuri,[1,2] Xiuquan Ma,[1,2] Scott Peterman,[4] David E. James[1,2,5]†

A major goal in signaling biology is the establishment of high-throughput quantitative methods for measuring changes in protein phosphorylation of entire signal transduction pathways across many different samples comprising temporal or dose data or patient samples. Data-independent acquisition (DIA) mass spectrometry (MS) methods, which involve tandem MS scans that are collected independently of precursor ion information and then are followed by targeted searching for known peptides, may achieve this goal. We applied DIA-MS to systematically quantify phosphorylation of components in the insulin signaling network in response to insulin as well as in stimulated cells exposed to a panel of kinase inhibitors targeting key downstream effectors in the network. We accurately quantified the effect of insulin on phosphorylation of 86 protein targets in the insulin signaling network using either stable isotope standards (SIS) or label-free quantification (LFQ) and mapped signal transmission through this network. By matching kinases to specific phosphorylation events (based on linear consensus motifs and temporal phosphorylation) to the quantitative phosphoproteomic data from cells exposed to inhibitors, we investigated predicted kinase-substrate relationships of AKT and mTOR in a targeted fashion. Furthermore, we applied this approach to show that AKT2-dependent phosphorylation of GAB2 promoted insulin signaling but inhibited epidermal growth factor (EGF) signaling in a manner dependent on 14-3-3 binding. Because DIA-MS can increase throughput and improve the reproducibility of peptide detection across multiple samples, this approach should facilitate more accurate, comprehensive, and quantitative assessment of signaling networks under various experimental conditions than are possible using other MS proteomic methods.

INTRODUCTION

Quantification of the flow of information through signaling pathways in response to environmental or pathological stimuli is vital for our understanding of cellular processes, health, and disease. Extraordinary improvements in mass spectrometry (MS) have transformed modern molecular biology, enabling scientists to routinely identify and quantify thousands of proteins in an unbiased manner. High-throughput proteome analysis of complex peptide mixtures can be achieved with several liquid chromatography–tandem MS (LC-MS/MS) methods, including "shotgun" proteomics (also called discovery proteomics) using data-dependent acquisition (DDA) and "targeted" proteomics using selected reaction monitoring (SRM). In DDA, the instrument consecutively isolates and fragments the most abundant precursor ions throughout the chromatographic separation. The fragmented precursor ions are then excluded from reisolation ("dynamic exclusion") for a fixed duration, thereby enabling precursors of lower abundance to be fragmented. This method is the most widely used strategy for untargeted identification and quantification, when the goal is rapid and complete proteome identification and quantification (*1*). However, despite great progress in the sensitivity and sequencing speeds of modern mass spectrometers, irreproducible detection of biologically important peptides in repeated analysis has thus far limited the application of this approach in routine clinical research or clinical diagnosis and prognosis (*2*–*5*). To circumvent these limitations, targeted MS acquisition methods such as SRM aim to reproducibly detect peptides across multiple samples (*6*). Targeted approaches such as SRM are well suited to accurate and reproducible quantification of a known set of peptides, yet the time required to develop the assay and the limited number of peptides that can be assayed have limited the widespread application of this approach to phosphorylation analysis (*7*). So far, the use of targeted proteomics to analyze the phosphorylation of multiple proteins across many samples has been limited (*8*–*11*). An alternative method termed "data-independent acquisition" (DIA) has been proposed, promising to maximize proteome depth, increase the reproducibility of analyte quantification, and increase throughput and simplify assay development. Various DIA methods [also called multiplexed tandem MS (*12*)] have been developed [for a comprehensive review, see (*13*)]. The major difference between these methods and DDA or SRM is the simultaneous co-isolation, co-fragmentation, and co-detection of multiple precursor ions. In DIA methods, ions entering the mass spectrometer over a specified mass/charge ratio (*m/z*) range are isolated together, and composite fragment ion spectra are generated without previous knowledge of the precursor ion masses. The major advantage of this approach is that all precursor ions present are subjected to MS/MS across a desired *m/z* range. This essentially generates a fragment ion record of the sample, and any peptide falling in the analyzed *m/z* range can theoretically be quantified, which should improve the reproducibility of peptide detection across multiple samples.

Here, we used DIA to systematically quantify phosphorylation of multiple components in the insulin signaling network in 3T3-L1 adipocytes. Our data revealed that label-free quantification–based DIA (LFQ-DIA) is a robust option for the measurement of signaling across many samples with low variability. To explore the extensibility of DIA data for analyzing signaling

[1]Charles Perkins Centre, School of Molecular Bioscience, University of Sydney, Sydney, New South Wales 2006, Australia. [2]Garvan Institute of Medical Research, Darlinghurst, New South Wales 2010, Australia. [3]Department of Proteomics and Signal Transduction, Max Planck Institute for Biochemistry, Martinsried 82152, Germany. [4]Thermo Fisher Scientific, Cambridge, MA 02139, USA. [5]School of Medicine, University of Sydney, Sydney, New South Wales 2006, Australia.
*These authors contributed equally to this work.
†Corresponding author. E-mail: david.james@sydney.edu.au

networks, we subsequently built a large phosphopeptide spectral library using shotgun proteomics (namely, DDA) and used this library to perform targeted data extraction (*14*) of our DIA data to quantify previously predicted AKT and mechanistic target of rapamycin (mTOR) substrates (*15*). Our data highlighted a complex, regulated phosphorylation of growth factor receptor–bound protein 2 (GRB2)–associated binding protein 2 (GAB2) in response to insulin stimulation in the presence of various inhibitors. In vitro kinase assays are a routine tool used by signal transduction researchers to investigate kinase-substrate relationships; however, they traditionally rely on the availability of phosphospecific antibodies or labor-intensive site-directed mutagenesis in combination with radioactive labeling. We posited that LFQ-DIA could be used as a rapid and quantitative readout of in vitro kinase assays to reveal site-specific phosphorylation. We tested this approach using GAB2 and found that AKT can directly phosphorylate GAB2 at Ser^{211} and Thr^{291}. Finally, we investigated the functional effects of GAB2 phosphorylation and highlighted a positive and negative feedback mechanism following insulin compared to epidermal growth factor (EGF) stimulation involving 14-3-3 binding. Together, this study demonstrates that DIA is an attractive strategy for the quantification of broad cellular signaling, permitting rapid assay development and a straightforward analysis pipeline.

RESULTS

Production of a stable isotope standard peptide library of known insulin-regulated phosphopeptides

We synthesized 15 phosphopeptides previously shown to be regulated by insulin in 3T3-L1 adipocytes using stable isotope labeling by amino acids in cell culture (SILAC)–based phosphoproteomics (*15*). These phosphorylation sites play essential roles in the regulation of diverse cellular functions (Fig. 1A). The phosphopeptides contained heavy-labeled Lys or Arg [stable isotope standard (SIS)]. Approximately equimolar amounts of heavy-labeled phosphopeptide mixtures were prepared and analyzed by DDA-MS, and the data were analyzed using Sequest HT, Percolator (*16*), and phosphoRS (*17*). We identified all 15 phosphopeptides, and phosphorylated residues were localized with >99% probability (table S1). We created a second SIS "balanced" phosphopeptide mixture so that the signal from each phosphopeptide was detected in the middle of the dynamic range of the mass spectrometer (meaning the intensity of the precursor ion was about 1×10^8).

Quantification of insulin signaling in the presence of inhibitors targeting central nodes in the network

We next investigated insulin-stimulated phosphorylation in differentiated 3T3-L1 adipocytes in the presence or absence of inhibitors targeting downstream effectors of the insulin signaling pathway. A total of 26 samples were prepared: basal, insulin treated, insulin and AKT inhibitor

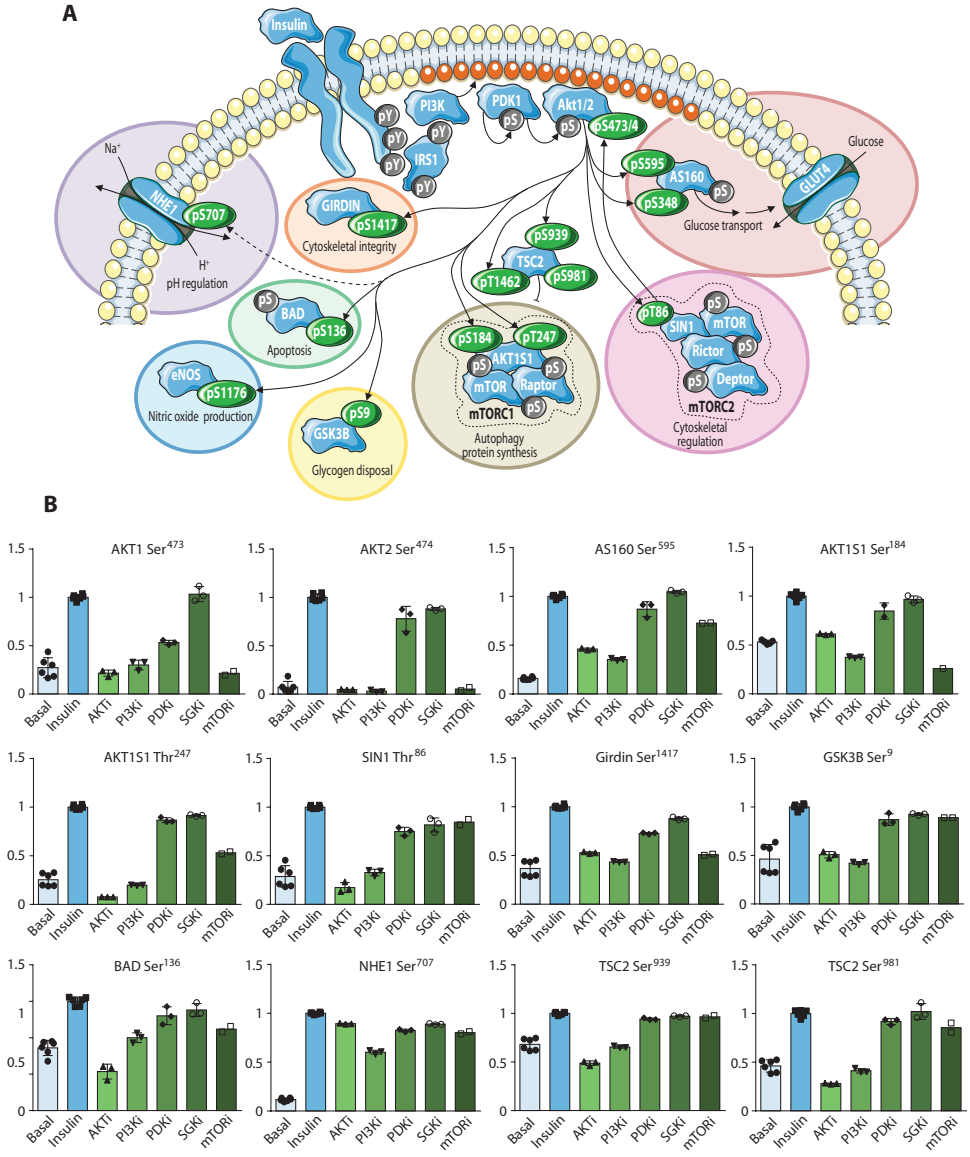

Fig. 1. Targeted quantification of insulin-stimulated phosphorylation of AKT substrates using SIS-DIA with kinase inhibition of key signaling nodes. (A) Insulin-regulated AKT substrates regulate diverse cellular functions. (B) Quantification of phosphopeptides using SIS-DIA in response to insulin in the presence or absence of kinase inhibition. 3T3-L1 adipocytes were subject to basal conditions ($n = 6$ biological replicates), insulin ($n = 6$ biological replicates), insulin and AKT inhibitor (AKTi) ($n = 3$ biological replicates), insulin and phosphatidylinositol 3-kinase (PI3K) inhibitor (PI3Ki) ($n = 3$ biological replicates), insulin and phosphoinositide-dependent protein kinase (PDK) inhibitor (PDKi) ($n = 3$ biological replicates), insulin and serum- and glucocorticoid-inducible kinase (SGK) inhibitor (SGKi) ($n = 3$ biological replicates), and insulin and mTOR inhibitor (mTORi) ($n = 2$ biological replicates). Source data and statistical analysis [Tukey one-way analysis of variance (ANOVA)] are shown in table S2.

Fig. 2. Targeted quantification of insulin-stimulated phosphorylation of predicted AKT and mTOR substrates using LFQ-DIA with kinase inhibition of key signaling nodes. Quantification of phosphopeptides using LFQ-DIA in response to insulin or insulin in the presence of kinase inhibition. 3T3-L1 adipocytes were subject to basal conditions (n = 6 biological replicates), insulin (n = 6 biological replicates), insulin and AKT inhibitor (n = 3 biological replicates), insulin and PI3K inhibitor (n = 3 biological replicates), insulin and PDK inhibitor (n = 3 biological replicates), insulin and SGK inhibitor (n = 3 biological replicates), and insulin and mTOR inhibitor (n = 2 biological replicates). Source data and statistical analysis (Tukey one-way ANOVA) are shown in table S4.

treated, insulin and PI3K inhibitor treated, insulin and PDK inhibitor treated, insulin and SGK inhibitor treated, and insulin and mTOR inhibitor treated. Cell lysates were digested and peptides were mixed with the balanced SIS phosphopeptide mixture. Phosphopeptides were enriched by TiO_2 chromatography, and the elution was analyzed directly by single-shot DIA-MS. Thirteen of the 15 endogenous phosphopeptides were identified on the basis of several stringent criteria, and models were trained using the mProphet algorithm (*18*) (fig. S1 and table S2). The signals for Ser^{1176} in endothelial nitric oxide synthase (eNOS) and Ser^{348} in AS160 were of low intensity and contained a low signal-to-noise ratio, and hence, they were not identified. Therefore, they were excluded from further analysis.

An investigation of the various strategies for quantification indicated that product ion extracted ion chromatograms (MS2) had the lowest average coefficient of variation (CV) of 5.6% in the insulin-stimulated group using LFQ compared with precursor ion extracted ion chromatograms (MS1) of 7.2% (fig. S2). This value was further reduced to an average CV of 2.5% with SIS phosphopeptide normalization. Insulin stimulation significantly increased the phosphorylation of all phosphopeptides investigated, validating previous SILAC-based quantification (*15*) (Fig. 1B and table S2). The insulin-stimulated phosphorylation of Ser^{473} in AKT1 and Ser^{474} in AKT2 was inhibited by more than 80% with AKT inhibition. Upstream inhibition of PI3K and mTOR also resulted in marked attenuation of insulin-stimulated phosphorylation of AKT; however, PDK1 inhibition only produced partial attenuation. Blockade of SGK did not significantly affect the phosphorylation of AKT or its substrates, consistent with its position downstream of AKT within the signaling network. The phosphorylation of insulin-regulated sites was potently decreased by AKT and PI3K inhibitors, with the exception of Ser^{707} in NHE1, which has been proposed to be phosphorylated by either p90 ribosomal protein S6 kinase (p90RSK) or extracellular signal–regulated kinases 1 and 2 (ERK1/2) (*19*) (Fig. 1B). This finding agrees with previous SILAC-based quantification (*15*). The phosphorylation of AKT substrates showed different sensitivities to mTOR inhibition. For example, mTOR inhibition blocked the phosphorylation of Ser^{184} in AKT1S1 (also known as PRAS40) and Ser^{1417} in Girdin, but not that of Ser^{9} in glycogen synthase kinase 3B (GSK3B) or of various phosphorylation sites on TSC2 (Fig. 1B). This finding was consistent with previous observations in mTORC2-deficient cells ($SIN1^{-/-}$ mouse embryonic fibroblasts), where the complete absence of AKT phosphorylation at Ser^{473} is accompanied by reduced phosphorylation of some AKT substrates without perturbing that of other substrates (*20*).

Targeted quantification of predicted AKT and mTOR substrate phosphorylation using label-free DIA

We next used spectral libraries and LFQ-DIA to quantify predicted substrates of AKT and mTOR (*15*). On the basis of previous predictions, a list of 60 top-ranked possible AKT and mTOR substrates was compiled. Ten control phosphopeptides, which are protein kinase A (PKA) substrates, were included in this list, and their phosphorylation was decreased in response to insulin. A list of 130 phosphosites was targeted in total. We next generated a spectral library containing 8561 phosphorylation sites (>90% phosphoRS localization) from 3T3-L1 adipocytes stimulated with insulin using DDA-MS (table S3). We used this library to screen the response of 130 phosphosites to insulin stimulation. Of these 130 phosphopeptides, we identified 98 phosphosites using DDA-MS. These data were used to perform targeted data extraction and reinterrogation of the DIA analysis acquired above. Phosphopeptide identification was performed using several criteria and mProphet (fig. S3), and on the basis of stringent filtering, 73 of the 98 phosphopeptides were identified in the DIA data (table S4). Of the 73 phosphopeptides identified, 57 phosphosites were localized on the basis of detectable fragment ions in the DIA data. A total of 10 phosphopeptides displayed more than one discrete elution profile originating from potential phosphosite localization isoforms, and 5 of these contained fragment ions for localization identical to the spectral library. MS2-based quantification resulted in an average CV of 8.9%, with 67 of the 73 phosphopeptides displaying <20% CV in the insulin-stimulated group. Insulin increased the abundance of 57 of the 73 targeted phosphopeptides (Fig. 2). AKT and PI3K inhibitors potently suppressed insulin-induced phosphorylation of most known AKT substrates and predicted substrates with high prediction scores, whereas lower-scoring predicted substrates tended to

be also affected by mTOR inhibition. The SGK inhibitor modestly inhibited phosphorylation of five substrates, and it potently inhibited phosphorylation of Ser[167] in T cell transcription factor EB. The insulin-stimulated phosphorylation of most known and predicted mTOR substrates was potently inhibited by AKT, PI3K, and mTOR inhibitors, consistent with the role of mTOR downstream of AKT and PI3K in the signaling network. The control phosphopeptides we analyzed correlated well with previous SILAC data, including the decreased phosphorylation of Ser[358] in SIK2, a PKA substrate.

AKT2-specific phosphorylation of GAB2 revealed by targeted quantification

We next wanted to apply the DIA method in a more focused experimental framework. Many signal transduction experiments involve analysis of multiple phosphorylation sites on one protein. To this end, we focused on the scaffold protein GAB2 because it acts downstream of various receptor tyrosine kinases including insulin-like growth factor receptor (IGFR) and EGF receptor (EGFR); however, little is known about its role in insulin signaling. Moreover, we have previously identified various insulin-regulated sites in GAB2 phosphorylation with SILAC (*15*). Analysis of the phosphorylation of GAB2 at Ser[211] (Ser[210] in the human form), Thr[388] (Thr[391] in the human form), and Ser[532] (Ser[543] in the human form) using LFQ-DIA confirmed their insulin-regulated phosphorylation and revealed that these phosphosites showed distinct responses to various inhibitors (Fig. 2 and table S4). EGF treatment of MCF-10A cells increases the phosphorylation of Ser[210] and Thr[391] in GAB2 and promotes its binding to 14-3-3 proteins (*21*). EGF-induced phosphorylation of these sites is attenuated with AKT and PI3K inhibition; however, only Ser[160] (Ser[159] in the human form) can be phosphorylated by AKT1 in vitro (*22*). These results suggest that either AKT2/3 isoforms or a downstream kinase catalyzes the phosphorylation of Ser[211] and Thr[388] in response to insulin. Although RSK phosphorylates GAB2 at Ser[160], Ser[211], and Ser[620] in human embryonic kidney (HEK) 293 cells stimulated with phorbol 12-myristate 13-acetate (PMA) or EGF (*23*), we found no evidence for insulin-dependent activation of RSK in 3T3-L1 fibroblasts or HEK293 cells (fig. S4). To investigate the possibility of AKT2-dependent phosphorylation of Ser[211] and Thr[388] sites, we performed an AKT2 in vitro kinase assay, using LFQ-DIA as a site-specific activity readout (fig. S5). Immunoprecipitated GAB2 was analyzed by DDA-MS (table S5). An in vitro AKT2 kinase assay, using immunoprecipitated GAB2 as a substrate, was subsequently analyzed by DIA-MS, and targeted data extraction of GAB2 peptides was performed (table S6). Incubation of GAB2 with AKT2 increased the phosphorylation of Ser[211] and Thr[388] by 19- and 16-fold for replicate 1, respectively, and by 3- and 2-fold for replicate 2, respectively (Fig. 3A), an increase that was almost completely abolished by the AKT kinase inhibitor GDC0068. Western blot analysis of the same samples using phosphospecific antibodies against Ser[211] and Thr[388] in GAB2 confirmed increased AKT2-mediated phosphorylation, an increase that was partially attenuated with GDC0068 (Fig. 3B). The fold change observed by immunoblotting with phosphospecific antibodies raised against these two sites did not match that obtained with LFQ-DIA. The reduced signal obtained with the phosphospecific antibodies is possibly caused by residual binding of the antibody to the nonphosphorylated epitope. Collectively, these results show that AKT2 can phosphorylate GAB2 at Ser[211] and Thr[388].

Differential effects of GAB2 phosphorylation at Ser[211] and Thr[388] on insulin and EGF signaling

Phosphorylation of GAB2 at Ser[211] and Thr[388] results in 14-3-3 binding and inhibits the interaction of GAB2 with GRB2, SHC, SHP2, and EGFR signaling complexes in MCF-10A cells. This interaction attenuates EGF-mediated AKT activation through a negative feedback mechanism (*21*). Consistent with previous studies, overexpression of wild-type GAB2 in 3T3-L1 fibroblasts and HEK293 cells potentiated EGF-dependent phosphorylation of AKT, and overexpression of a GAB2 phosphomutant containing alanine substitutions at Ser[211] and Thr[388] (GAB2-2A) further increased phosphorylation of AKT (Fig. 3, C and D) (*21*). These effects were rescued by overexpression of a GAB2 mutant (GAB2-2R18) that constitutively binds to 14-3-3 proteins (Fig. 3, C and D). In contrast, overexpression of wild-type GAB2 in 3T3-L1 fibroblasts inhibited insulin-stimulated phosphorylation of AKT but had no effect in HEK293 cells. Overexpression of the GAB2-2A mutant inhibited insulin-stimulated AKT phosphorylation in both 3T3-L1 fibroblasts and HEK293 cells. This inhibitory effect was reversed by overexpression of the 14-3-3–binding GAB2 mutant (Fig. 3, C and D). These results suggest that phosphorylation of GAB2 at Ser[211] and Thr[388] and subsequent binding of 14-3-3 promotes insulin-induced phosphorylation of AKT but suppresses EGF-induced AKT phosphorylation. A similar inverse relationship for the effects of GAB2 on insulin and EGF was observed for the AKT substrate Thr[246] in PRAS40 and the mTOR substrate Thr[389] in p70S6K (Fig. 3, C and D).

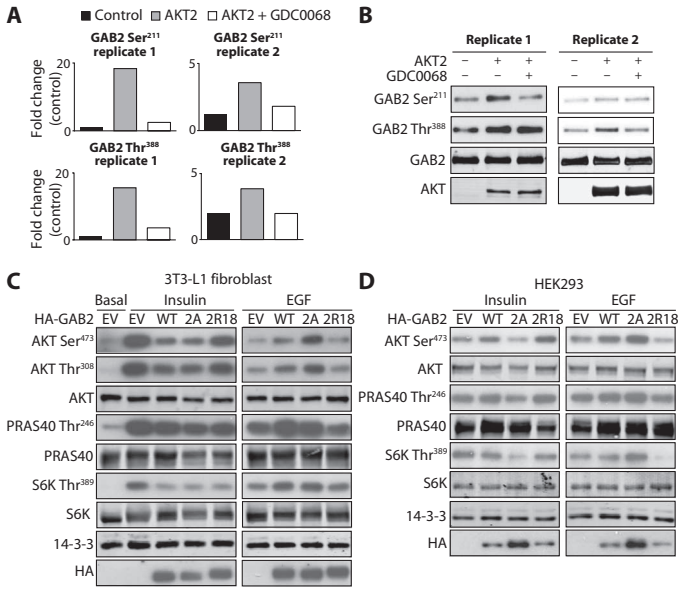

Fig. 3. AKT2-dependent phosphorylation of GAB2 at Ser[211] and Thr[388] enhances insulin signaling and suppresses EGF signaling. (**A**) Quantification of GAB2 phosphopeptides containing Ser[211] and Thr[388] (n = 2 biological replicates). (**B**) Western blot analysis of AKT2 in vitro kinase assay using immunoprecipitated GAB2 and blotted with the indicated antibodies (n = 2 biological replicates). (C and D) 3T3-L1 fibroblasts (**C**) or HEK293 cells (**D**) overexpressing hemagglutinin (HA)–tagged GAB2 (EV, empty vector; WT, wild-type; 2A, S211A and T388A; 2R18, 14-3-3–binding peptide at Ser[211] and Thr[388]) stimulated with insulin or EGF and blotted with the indicated antibodies (n = 2 biological replicates).

DISCUSSION

Here, we applied DIA-MS to quantify signal transduction through the insulin signaling network in adipocytes. We could simultaneously quantify insulin-dependent changes in the phosphorylation of 69 different

proteins, as well as their response to a suite of small-molecule kinase inhibitors. This method is more rapid than other methods, such as immunoblotting or SRM, and should afford researchers' greater flexibility in studying signal transduction under a range of experimental conditions. We also applied the method to study changes in phosphorylation of a single regulatory node—GAB2—and unveiled signal regulatory properties of this node in response to different growth factors.

DIA-MS offers several advantages compared to other targeted acquisition methods, such as SRM. First, the fragmentation of every precursor ion over a specified *m/z* range circumvents the need to select peptides and optimize the transitions, and the fragmentation of all precursors means that DIA data can theoretically be subsequently reinterrogated to extract quantitative information about peptides of interest. One caveat to this approach is that reduced dynamic range and sensitivity compared with SRM approaches will limit the ability to perform targeted data extraction (*14*). Previous evaluations of DIA with large isolation windows have used samples of limited complexity such as bacteria and yeast (*14*, *24*, *25*) or immunoprecipitations (*26*–*28*). The use of single-shot DIA with large isolation windows to quantify peptides of extremely low abundance in complex mammalian whole-cell lysates may not be suitable. However, the reduction in sample complexity with phosphopeptide enrichment overcomes these limitations. Here, we used single-shot DIA-MS for targeted phosphoproteomics analysis of signaling networks, focusing on insulin signaling. We initially targeted 15 phosphopeptides using spike-in–labeled peptides and found that quantification with MS2 outperforms MS1-based quantification, most likely due to the additional level of specificity of MS2 ions and the previously observed increase in signal-to-noise conferred (*29*). A simplified balancing of the amount of labeled peptides, followed by spiking this mixture into a suitable amount of starting material for single-shot LC-MS/MS, facilitated rapid assay development in combination with the ease of DIA. We also investigated LFQ of these 15 phosphopeptides and showed that low variance (<20% CV) was achievable for samples processed on the same day without any normalization. Presenting signaling data as fold change (stimulus compared to control) facilitated comparison of results from experiments performed on different days for most of the phosphopeptides. Furthermore, the effect of kinase inhibition in the presence of insulin was effectively determined by presenting the data as a percentage of inhibition relative to insulin alone, namely, a minimum/maximum where unstimulated was set to 0% and insulin to 100%. More elaborate normalization methods would likely be required if these minimum/maximum measurements were not made on each day (*27*). We further show the strength of phosphoproteomics analysis using LFQ-DIA by subsequently building spectral libraries with DDA and then reinterrogating the DIA data to investigate key signaling molecules of interest from a previous study. Such targeted data extraction permitted rapid testing of additional hypotheses, such as whether previously predicted substrates are sensitive to pharmacological compounds not included in the original screen. However, the ability to target a curated list of phosphopeptides is dependent on identification using spectral libraries and/or SIS. We initially quantified 13 of the 15 targeted phosphopeptides downstream of AKT using SIS, and 73 of 130 phosphopeptides predicted downstream targets of AKT, mTOR, or PKA using LFQ. Further analysis on instruments with improved transmission and sensitivity, such as the Q Exactive HF (*30*), or acquisition strategies with improved specificity (*29*) will likely increase the fraction of targeted phosphopeptides identified. Together, these results demonstrate that single-shot DIA-MS is a viable strategy for targeted phosphoproteomics. The approach showed low variation and data acquisition was relatively straightforward, making this an attractive avenue for future clinical phosphoproteomic analyses.

We used LFQ-DIA to investigate kinase-substrate relationships and show that AKT2 phosphorylates GAB2 at Ser^{211} and Thr^{388} in vitro. Both insulin and EGF promote GAB2 phosphorylation at multiple sites in various cell types. RSK phosphorylates GAB2 at Ser^{160}, Ser^{211}, and Ser^{620} (Ser^{631} human) in response to EGF and Ras/mitogen-activated protein kinase (MAPK) activation (*23*). However, insulin does not promote RSK phosphorylation and activation in 3T3-L1 fibroblasts or HEK293 cells (fig. S4), suggesting that GAB2 is phosphorylated by either AKT or RSK at these sites depending on the growth factor stimulation. We investigated the functional effects of AKT2-dependent phosphorylation of GAB2 and demonstrated a role of GAB2 phosphorylation as an inhibitor of EGF signaling. In contrast, GAB2 phosphorylation at Ser^{211} and Thr^{388} and subsequent binding of 14-3-3 mediated positive feedback regulation of insulin signaling. Although the precise mechanism of this differential regulatory effect is incompletely understood, both insulin and EGF can trigger GAB2 phosphorylation on Ser^{211} and/or Thr^{388} and subsequent recruitment of 14-3-3. One hypothesis could include the modulation of GAB2 adaptor complex stability. Binding of 14-3-3 promotes dissociation of GAB2 from GRB2 or p85 and thus termination of downstream GAB2 signaling. Alternatively, dissociated GAB2 may allow other adaptor complexes to form including p85 or insulin receptor substrates and thus serve as a positive feedback mechanism to promote insulin signaling. It is likely that these mechanisms are further controlled by the local concentrations, stoichiometry, and subcellular distributions of these adaptor molecules with various receptor tyrosine kinases. Further research is required to pinpoint the exact mechanism; however, this exciting observation may represent a fundamental regulatory node to drive different functional outcomes downstream of different growth factors.

The quantification of global phosphorylation across multiple samples is an attractive research tool to investigate aberrant signal transduction in developmental or disease processes. We show that phosphoproteomic analysis using DIA is an alternative to current MS-based strategies to allow cheap and rapid assay design. We believe that the use of this technology has great potential to drive further clinical research or therapeutic screening over a broad range of applications.

MATERIALS AND METHODS

Cell culture, plasmids, and antibodies

3T3-L1 fibroblasts and HEK293E were grown in Dulbecco's modified Eagle's medium (DMEM) supplemented with 10% fetal calf serum and 2 mM L-alanyl-L-glutamine in 10% CO_2 at 37°C. For 3T3-L1 fibroblasts, confluent cells were differentiated into adipocytes as previously described (*31*) and used 10 or 12 days after differentiation. To establish basal conditions before analysis, cells were incubated in serum-free DMEM for 2 hours in 10% CO_2 at 37°C. Cells were stimulated with either insulin (100 nM), EGF (50 ng/ml), or PMA (250 ng/ml) as specified for 10 or 20 min. For inhibitor experiments, cells were treated for 30 min at the end of the baseline period with the following inhibitors: MK2206 (10 nM; AKT inhibitor), LY294002 (50 nM; PI3K inhibitor), GSK2334470 (1 μM; PDK inhibitor), GSK650394 (1 μM; SGK inhibitor), torin 1 (250 nM; mTOR inhibitor), U0126 (10 μM, MAPK kinase inhibitor), and PF4708671 (10 μM, S6K inhibitor). For analysis of 3T3-L1 adipocytes by DIA-MS, a total of 26 samples were prepared across two separate days: experiment 1 (10 days after differentiation)—basal ($n = 3$), insulin ($n = 3$), AKT inhibitor ($n = 3$), and PI3K inhibitor ($n = 3$); experiment 2 (12 days after differentiation)—basal ($n = 3$), insulin ($n = 3$), PDK inhibitor ($n = 3$), SGK inhibitor ($n = 3$), and mTOR inhibitor ($n = 2$). For transient transfection, cells at 50% confluence were incubated with 2.5:1 Lipofectamine 2000/plasmid DNA ratio in Opti-MEM for 24 hours and assayed 48 hours after transfection. The pMIG-GAB2-HA constructs (wild-type, 2A, and 2R18) and polyclonal anti–phospho-Ser^{211} and anti–phospho-Thr^{388} antibodies used in this study were from R. Daly (Monash University). For generation of p3×FLAG-Gab2,

the full-length human Gab2 complementary DNA was moved from pMIG-Gab2-HA to p3×FLAG-CMV gateway vector by LR recombination reaction.

Heavy-labeled phosphopeptide synthesis

The internal standards used for phosphopeptide quantification were obtained from Thermo Fisher Scientific GmbH. The collection of Thermo Scientific PEPotec SRM Peptide Libraries was synthesized with the specific site of phosphorylation and isotopic enrichment on the basis of endogenous peptide sequencing. Each synthetic peptide was evaluated using MS before shipping and confirmed at levels in excess of 0.1 mg in 1:1:0.1 water/acetonitrile (MeCN)/trifluoroacetic acid (TFA). A standard mixture of the SIS phosphopeptides was created from the individual stock solution and evaluated separately by identical LC-MS on the Q Exactive mass spectrometer as that for the biological samples. A static amount of the SIS mixture was then spiked into each of the digested samples before phosphopeptide enrichment.

Cell lysis, peptide preparation, and phosphopeptide enrichment

3T3-L1 adipocytes were lysed in 6 M urea, 2 M thiourea, 25 mM triethylammonium bicarbonate (pH 7.5), containing protease and phosphatase inhibitor cocktails (Roche), followed by a 10-s tip-probe sonication. Cellular debris was removed by centrifugation at 16,000*g* for 15 min, and protein concentration was determined using Qubit (Invitrogen) in triplicate. For the single-shot phosphoproteomic analysis by DIA, protein was normalized to 260 μg and reduced with 10 mM dithiothreitol for 60 min at 25°C followed by alkylation with 25 mM iodoacetamide for 30 min at 25°C in the dark. The reaction was quenched to a final concentration of 20 mM dithiothreitol and digested with Lys-C (Wako) at 1:50 enzyme/substrate ratio for 2 hours at 25°C. The mixture was diluted fivefold with 25 mM triethylammonium bicarbonate and digested with trypsin at 1:50 enzyme/substrate ratio for 12 hours at 30°C. The peptide mixture was acidified to a final concentration of 2% formic acid and centrifuged at 16,000*g* for 15 min. Peptides were desalted using 100 mg of tC18 cartridges followed by elution with 50% MeCN, 0.1% TFA and dried by vacuum centrifugation. Peptides were resuspended in 500 μl of titanium dioxide loading buffer (1 M glycolic acid, 80% MeCN, 5% TFA) and spiked with balanced amount of heavy-labeled phosphopeptides (about 250 fmol per 2.5 μl). A slurry of titanium dioxide (2 mg in 50 μl of MeCN) was accurately added to the peptide mixture and rotated at room temperature for 20 min. The mixture was centrifuged at 10,000*g* for 1 min, and the beads were washed with 100 μl of titanium dioxide loading buffer followed by 80% MeCN, 2% TFA and finally 16% MeCN, 0.4% TFA. The beads were dried briefly by vacuum centrifugation and eluted with 50 μl of 1% ammonium hydroxide by shaking at room temperature for 15 min. The titanium dioxide elution slurry was loaded onto a C8-plugged microcolumn and eluted with gentle air pressure to trap beads. The beads were eluted with an additional 50 μl of 1% ammonium hydroxide, and the elution was pooled. Enriched phosphopeptides were acidified to a final concentration of 10% formic acid, 0.1% TFA, and desalted using C18 microcolumns. For the multidimensional phosphoproteomic analysis by DDA, 3 mg of protein was reduced, alkylated, and digested as described above. Phosphopeptide enrichment and separation into eight fractions using microhydrophilic interaction liquid chromatography (microHILIC) was performed as described previously (*32*).

Mass spectrometry

Peptides were resuspended in 2% MeCN, 0.5% acetic acid and loaded onto a 50-cm × 75-μm inner diameter column packed in-house with 1.9-μm C18AQ particles (Dr. Maisch HPLC GmbH) using an Easy nLC-1000 UHPLC operated in single column mode with intelligent flow control loading at 950 bar. Peptides were separated using a linear gradient of 5 to 30% buffer B over 100 min at 250 nl/min (buffer A = 0.5% acetic acid; buffer B = 80% MeCN, 0.5% acetic acid). The column was maintained at 50°C using a PRSO-V1 ion source (Sonation) coupled directly to a Q Exactive mass spectrometer. For DDA, a full-scan MS1 was measured at 70,000 resolution at 200 *m/z* [300 to 1750 *m/z*; 100-ms injection time; 3×10^6 automated gain control (AGC) target] followed by isolation of up to 20 most abundant precursor ions for MS/MS (2 *m/z* isolation; 8.3×10^5 intensity threshold; 30.0 normalized collision energy; 17,500 resolution at 200 *m/z*; 60-ms injection time; 5×10^5 AGC target). For DIA, a full-scan MS1 was measured at 140,000 resolution at 200 *m/z* (300 to 1600 *m/z*; 120-ms injection time; 3×10^6 AGC target) followed by 16 × 25 *m/z* isolations and MS/MS from 450 to 850 *m/z* with a loop count of 8, that is, an intermittent MS1 scan after eight MS/MS (30.0 normalized collision energy; 17,500 resolution at 200 *m/z*; 60-ms injection time; 3×10^6 AGC target). Window placement was optimized in Skyline (*33*) to result in an inclusion list starting at 462.9603 *m/z* with increments of 25.0114 *m/z*.

Data processing and analysis

All DDA data were processed using Proteome Discoverer v1.4 and searched with Sequest HT against the mouse UniProt database (July 2013; 50,808 entries). The data were searched with methionine oxidation and serine, threonine, and tyrosine phosphorylation as variable modifications and carbamidomethylation of cysteine as a fixed modification using a precursor ion mass tolerance of 20 ppm and product ion mass tolerance of 0.02 dalton. All results were filtered to 1% false discovery rates (FDRs) using Percolator (*16*), and phosphosite localization was performed using phosphoRS (*17*). All DIA data were processed using Skyline v2.5.0.6157. Spectral libraries were built in Skyline with .msf files using the BiblioSpec algorithm (*34*). Precursor and product ion extraction ion chromatograms (XICs) were generated using extraction windows twofold the full width at half-maximum for both MS1 and MS2 filtering. Ion match tolerance was set to 0.055 *m/z* and matched to charges 2+, 3+, and 4+ for MS1 filtering of the first three isotopic peaks and 1^+, 2+, and 3+ for MS2 filtering of b- and y-type ions. Peak scoring models were trained on the basis of mProphet (*14*) and OpenSWATH (*35*) using a combination of scores and filtered to 1% FDR. For the analysis of phosphopeptides containing SIS, the model was trained using the following criteria: (i) library intensity dot product (dot product between library spectrum and light phosphopeptide), (ii) reference intensity dot product (dot product between light and heavy phosphopeptides), (iii) co-elution count (number of co-eluting light phosphopeptide transitions), and (iv) reference co-elution count (number of co-eluting heavy phosphopeptide transitions). These were used to rescore peak picking and peak integration boundaries as described in the *Advanced Peaking Picking Models* tutorial (https://skyline.gs.washington.edu/labkey/wiki/home/software/Skyline/page.view?name=tutorial_peak_picking). These were then further analyzed manually, and correct identification was assigned on the basis of the following criteria: (i) retention time matching to spectral library within 5% of the gradient length, (ii) co-elution of light and heavy phosphopeptides within 0.01 min, (iii) dot product between light phosphopeptide precursor ion isotope distribution intensities and theoretical >0.95, (iv) dot product between library spectrum intensities and light phosphopeptides >0.90, and (v) matching peak shape for precursor and product ions from light and heavy phosphopeptides. For the label-free analysis of phosphopeptides, the model was trained using the following criteria: (i) library intensity dot product (dot product between library spectrum and light phosphopeptide) and (ii) co-elution count (number of co-eluting light phosphopeptide transitions). These were then further analyzed manually, and correct identification was assigned on the basis of the following criteria: (i) retention time matching to spectral library within 5% of the gradient

length, (ii) dot product between light phosphopeptide precursor ion isotope distribution intensities and theoretical >0.95, (iii) dot product between library spectrum intensities and light phosphopeptides >0.90, and (iv) matching peak shape for precursor and product ions from light phosphopeptides. Phosphosite localization in the DIA data was manually performed on the basis of diagnostic fragment ions in the spectral library. Additionally, manual interrogation of MS1 XIC enabled the identification of isobaric phosphopeptides with differing phosphosite localizations and discrete elution profiles. DIA data of the insulin stimulation and inhibitor screen were normalized for each experiment expressed relative to the average insulin stimulation. This was effectively achieved by including a basal and insulin simulation in both experiments and setting these as the minimum and maximum response. The effect of kinase inhibition in each separate experiment was compared to this response and expressed as a percentage. This overcame differences in total area sums of each replicate between the two experiments (table S7). Statistical analysis was performed in GraphPad Prism. Data visualization was performed in R programming environment (R Core Team, *R: A Language and Environment for Statistical Computing*, R Foundation for Statistical Computing, Vienna, Austria, 2014; http://www.R-project.org/) using library corrplot (T. Wei, *corrplot: Visualization of a Correlation Matrix*, R package version 0.73, 2013; http://CRAN.R-project.org/package=corrplot). Data were preprocessed and scaled [all nonsignificant inhibitions ($P > 0.05$) were set at an artificial maximum value] such that sites with significantly increased and decreased inhibition were color-coded in red and blue, respectively, whereas nonsignificant inhibitions were rendered in gray and removed. The magnitude of inhibition (%) is represented by the size of the circles in the matrix.

AKT2 in vitro kinase assay

HEK293E cells were transiently transfected with human FLAG-tagged GAB2 and serum-starved for 2 hours. Cells were treated with either insulin (100 nM; 20 min) for DDA analysis and spectral library generation or wortmannin (100 nM; 30 min) for AKT2 kinase assay and DIA analysis. Cells were lysed in NP-40 buffer [1% NP-40, 150 mM NaCl, 50 mM tris-HCl, 10% glycerol, protease and phosphatase inhibitor cocktail (pH 7.4)] using a 22-gauge needle 10 times followed by a 27-gauge needle 3 times. Cellular debris was removed by centrifugation at 16,000*g* for 10 min, and protein concentration was determined using bicinchoninic acid assay. A 30-µl slurry of protein G Sepharose (GE Life Sciences) was resuspended in 500 µl of NP-40 buffer and incubated with 2 µg of monoclonal anti-FLAG M2 antibody (Sigma) for 2 hours at 4°C with rotation. The beads were washed briefly with NP-40 buffer and incubated with 2 mg of protein lysate to immunoprecipitate FLAG-tagged GAB2 for 2 hours at 4°C. The beads were washed three times with NP-40 buffer and once with phosphate-buffered saline (PBS). Excess PBS was removed with a 20-µl GELoader tip, and the beads were resuspended in 40 µl of kinase buffer [25 mM tris-HCl, 10 mM $MgCl_2$, 5 mM β-glycerophosphate, 2 mM dithiothreitol, 400 µM adenosine triphosphate (pH 7.4)] containing 15 µg of 3×FLAG peptide (Sigma) to elute FLAG-tagged GAB2. Kinase reactions were performed with 200 ng of AKT2 (Cell Signaling; replicate 1) or 10 U of AKT2 (SignalChem; replicate 2) for 20 min at 37°C and quenched with 2 × SDS–polyacrylamide gel electrophoresis loading buffer.

SUPPLEMENTARY MATERIALS

www.sciencesignaling.org/cgi/content/full/8/380/rs6/DC1

Fig. S1. mProphet FDR of insulin-regulated phosphopeptides in 3T3-L1 adipocytes analyzed with DIA-MS and SIS.

Fig. S2. CV comparisons.

Fig. S3. mProphet FDR of insulin-regulated phosphopeptides in 3T3-L1 adipocytes analyzed with DIA-MS and LFQ.

Fig. S4. PMA and EGF, but not insulin, promote the phosphorylation and activation of RSK.

Fig. S5. Strategy for in vitro kinase analysis of immunoprecipitated FLAG-tagged GAB2 using DIA-MS.

Table S1. Identification of synthetic heavy-labeled phosphopeptides by DDA-MS.

Table S2. Targeted quantification of insulin-regulated phosphopeptides in 3T3-L1 adipocytes after inhibitor treatment using DIA-MS and SIS.

Table S3. Identification of phosphopeptides in 3T3-L1 adipocytes using DDA-MS.

Table S4. Targeted quantification of insulin-regulated phosphopeptides in 3T3-L1 adipocytes after inhibitor treatment using DIA-MS and LFQ.

Table S5. Identification of immunoprecipitated FLAG-tagged GAB2 using DDA-MS.

Table S6. Quantification of immunoprecipitated FLAG-tagged GAB2 subjected to an AKT2 in vitro kinase assay using DIA-MS and LFQ.

Table S7. Total area sum of DIA analysis shown in tables S2 and S4.

REFERENCES AND NOTES

1. M. Mann, N. A. Kulak, N. Nagaraj, J. Cox, The coming age of complete, accurate, and ubiquitous proteomes. *Mol. Cell* **49**, 583–590 (2013).
2. A. Michalski, J. Cox, M. Mann, More than 100,000 detectable peptide species elute in single shotgun proteomics runs but the majority is inaccessible to data-dependent LC–MS/MS. *J. Proteome Res.* **10**, 1785–1793 (2011).
3. M. Berg, A. Parbel, H. Pettersen, D. Fenyö, L. Björkesten, Reproducibility of LC-MS-based protein identification. *J. Exp. Bot.* **57**, 1509–1514 (2006).
4. D. Stalder, A. Haeberli, M. Heller, Evaluation of reproducibility of protein identification results after multidimensional human serum protein separation. *Proteomics* **8**, 414–424 (2008).
5. E. Nouri-Nigjeh, S. Sukumaran, C. Tu, J. Li, X. Shen, X. Duan, D. C. DuBois, R. R. Almon, W. J. Jusko, J. Qu, Highly multiplexed and reproducible ion-current-based strategy for large-scale quantitative proteomics and the application to protein expression dynamics induced by methylprednisolone in 60 rats. *Anal. Chem.* **86**, 8149–8157 (2014).
6. V. Lange, P. Picotti, B. Domon, R. Aebersold, Selected reaction monitoring for quantitative proteomics: A tutorial. *Mol. Syst. Biol.* **4**, 222 (2008).
7. B. Domon, R. Aebersold, Options and considerations when selecting a quantitative proteomics strategy. *Nat. Biotechnol.* **28**, 710–721 (2010).
8. A. Wolf-Yadlin, S. Hautaniemi, D. A. Lauffenburger, F. M. White, Multiple reaction monitoring for robust quantitative proteomic analysis of cellular signaling networks. *Proc. Natl. Acad. Sci. U.S.A.* **104**, 5860–5865 (2007).
9. R. Narumi, T. Murakami, T. Kuga, J. Adachi, T. Shiromizu, S. Muraoka, H. Kume, Y. Kodera, M. Matsumoto, K. Nakayama, Y. Miyamoto, M. Ishitobi, H. Inaji, K. Kato, T. Tomonaga, A strategy for large-scale phosphoproteomics and SRM-based validation of human breast cancer tissue samples. *J. Proteome Res.* **11**, 5311–5322 (2012).
10. A. M. Zawadzka, B. Schilling, M. P. Cusack, A. K. Sahu, P. Drake, S. J. Fisher, C. C. Benz, B. W. Gibson, Phosphoprotein secretome of tumor cells as a source of candidates for breast cancer biomarkers in plasma. *Mol. Cell. Proteomics* **13**, 1034–1049 (2014).
11. M. P. Lam, S. B. Scruggs, T.-Y. Kim, C. Zong, E. Lau, D. Wang, C. M. Ryan, K. F. Faull, P. Ping, An MRM-based workflow for quantifying cardiac mitochondrial protein phosphorylation in murine and human tissue. *J. Proteomics* **75**, 4602–4609 (2012).
12. C. Masselon, G. A. Anderson, R. Harkewicz, J. E. Bruce, L. Pasa-Tolic, R. D. Smith, Accurate mass multiplexed tandem mass spectrometry for high-throughput polypeptide identification from mixtures. *Anal. Chem.* **72**, 1918–1924 (2000).
13. J. D. Chapman, D. R. Goodlett, C. D. Masselon, Multiplexed and data-independent tandem mass spectrometry for global proteome profiling. *Mass Spectrom. Rev.* **33**, 452–470 (2013).
14. L. C. Gillet, P. Navarro, S. Tate, H. Röst, N. Selevsek, L. Reiter, R. Bonner, R. Aebersold, Targeted data extraction of the MS/MS spectra generated by data-independent acquisition: A new concept for consistent and accurate proteome analysis. *Mol. Cell. Proteomics* **11**, O111.016717 (2012).
15. S. J. Humphrey, G. Yang, P. Yang, D. J. Fazakerley, J. Stöckli, J. Y. Yang, D. E. James, Dynamic adipocyte phosphoproteome reveals that Akt directly regulates mTORC2. *Cell Metab.* **17**, 1009–1020 (2013).
16. L. Käll, J. D. Canterbury, J. Weston, W. S. Noble, M. J. MacCoss, Semi-supervised learning for peptide identification from shotgun proteomics datasets. *Nat. Methods* **4**, 923–925 (2007).
17. T. Taus, T. Köcher, P. Pichler, C. Paschke, A. Schmidt, C. Henrich, K. Mechtler, Universal and confident phosphorylation site localization using phosphoRS. *J. Proteome Res.* **10**, 5354–5362 (2011).
18. L. Reiter, O. Rinner, P. Picotti, R. Hüttenhain, M. Beck, M.-Y. Brusniak, M. O. Hengartner, R. Aebersold, mProphet: Automated data processing and statistical validation for large-scale SRM experiments. *Nat. Methods* **8**, 430–435 (2011).
19. S. Chen, C. Mackintosh, Differential regulation of NHE1 phosphorylation and glucose uptake by inhibitors of the ERK pathway and p90RSK in 3T3-L1 adipocytes. *Cell. Signal.* **21**, 1984–1993 (2009).

20. E. Jacinto, V. Facchinetti, D. Liu, N. Soto, S. Wei, S. Y. Jung, Q. Huang, J. Qin, B. Su, SIN1/MIP1 maintains rictor-mTOR complex integrity and regulates Akt phosphorylation and substrate specificity. *Cell* **127**, 125–137 (2006).
21. T. Brummer, M. Larance, M. T. Herrera Abreu, R. J. Lyons, P. Timpson, C. H. Emmerich, E. D. G. Fleuren, G. M. Lehrbach, D. Schramek, M. Guilhaus, D. E. James, R. J. Daly, Phosphorylation-dependent binding of 14-3-3 terminates signalling by the Gab2 docking protein. *EMBO J.* **27**, 2305–2316 (2008).
22. D. K. Lynch, R. J. Daly, PKB-mediated negative feedback tightly regulates mitogenic signalling via Gab2. *EMBO J.* **21**, 72–82 (2002).
23. X. Zhang, G. Lavoie, L. Fort, E. L. Huttlin, J. Tcherkezian, J. A. Galan, H. Gu, S. P. Gygi, S. Carreno, P. P. Roux, Gab2 phosphorylation by RSK inhibits Shp2 recruitment and cell motility. *Mol. Cell. Biol.* **33**, 1657–1670 (2013).
24. J. D. Venable, M.-Q. Dong, J. Wohlschlegel, A. Dillin, J. R. Yates III, Automated approach for quantitative analysis of complex peptide mixtures from tandem mass spectra. *Nat. Methods* **1**, 39–45 (2004).
25. C. R. Weisbrod, J. K. Eng, M. R. Hoopmann, T. Baker, J. E. Bruce, Accurate peptide fragment mass analysis: Multiplexed peptide identification and quantification. *J. Proteome Res.* **11**, 1621–1632 (2012).
26. T. Geiger, J. Cox, M. Mann, Proteomics on an Orbitrap benchtop mass spectrometer using all-ion fragmentation. *Mol. Cell. Proteomics* **9**, 2252–2261 (2010).
27. J.-P. Lambert, G. Ivosev, A. L. Couzens, B. Larsen, M. Taipale, Z.-Y. Lin, Q. Zhong, S. Lindquist, M. Vidal, R. Aebersold, T. Pawson, R. Bonner, S. Tate, A.-C. Gingras, Mapping differential interactomes by affinity purification coupled with data-independent mass spectrometry acquisition. *Nat. Methods* **10**, 1239–1245 (2013).
28. B. C. Collins, L. C. Gillet, G. Rosenberger, H. L. Röst, A. Vichalkovski, M. Gstaiger, R. Aebersold, Quantifying protein interaction dynamics by SWATH mass spectrometry: Application to the 14-3-3 system. *Nat. Methods* **10**, 1246–1253 (2013).
29. J. D. Egertson, A. Kuehn, G. E. Merrihew, N. W. Bateman, B. X. MacLean, Y. S. Ting, J. D. Canterbury, D. M. Marsh, M. Kellmann, V. Zabrouskov, C. C. Wu, M. J. MacCoss, Multiplexed MS/MS for improved data-independent acquisition. *Nat. Methods* **10**, 744–746 (2013).
30. R. A. Scheltema, J. P. Hauschild, O. Lange, D. Hornburg, E. Denisov, E. Damoc, A. Kuehn, A. Makarov, M. Mann, The Q Exactive HF, a Benchtop mass spectrometer with a pre-filter, high-performance quadrupole and an ultra-high-field Orbitrap analyzer. *Mol. Cell. Proteomics* **13**, 3698–3708 (2014).
31. A. M. Shewan, B. J. Marsh, D. R. Melvin, S. Martin, G. W. Gould, D. E. James, The cytosolic C-terminus of the glucose transporter GLUT4 contains an acidic cluster endosomal targeting motif distal to the dileucine signal. *Biochem. J.* **350**, 99–107 (2000).
32. K. Engholm-Keller, P. Birck, J. Størling, F. Pociot, T. Mandrup-Poulsen, M. R. Larsen, TiSH—A robust and sensitive global phosphoproteomics strategy employing a combination of TiO_2, SIMAC, and HILIC. *J. Proteomics* **75**, 5749–5761 (2012).
33. B. MacLean, D. M. Tomazela, N. Shulman, M. Chambers, G. L. Finney, B. Frewen, R. Kern, D. L. Tabb, D. C. Liebler, M. J. MacCoss, Skyline: An open source document editor for creating and analyzing targeted proteomics experiments. *Bioinformatics* **26**, 966–968 (2010).
34. B. Frewen, M. J. MacCoss, Using BiblioSpec for creating and searching tandem MS peptide libraries. *Curr. Protoc. Bioinformatics* **Chapter 13**, Unit 13.7 (2007).
35. H. L. Röst, G. Rosenberger, P. Navarro, L. Gillet, S. M. Miladinović, O. T. Schubert, W. Wolski, B. C. Collins, J. Malmström, L. Malmström, R. Aebersold, OpenSWATH enables automated, targeted analysis of data-independent acquisition MS data. *Nat. Biotechnol.* **32**, 219–223 (2014).
36. V. Sharma, J. Eckels, G. K. Taylor, N. J. Shulman, A. B. Stergachis, S. A. Joyner, P. Yan, J. R. Whiteaker, G. N. Halusa, B. Schilling, B. W. Gibson, C. M. Colangelo, A. G. Paulovich, S. A. Carr, J. D. Jaffe, M. J. MacCoss, B. MacLean, Panorama: A targeted proteomics knowledge base. *J. Proteome Res.* **13**, 4205–4210 (2014).

Acknowledgments: We thank J. Egerston, B. MacLean, and R. Viner for the help setting up DIA methods, assistance with software, and useful discussions, and R. Daly for providing GAB2 constructs and antibodies. **Funding:** This work is supported by a National Health and Medical Research Council (NHMRC) program grant (D.E.J.). D.E.J. is an NHMRC Senior Principal Research Fellow. B.L.P. and G.Y. are recipients of an NHMRC Early Career Fellowship, and S.J.H. is a recipient of a European Molecular Biology Organization Long-Term Fellowship. The contents of the published material are solely the responsibility of the authors and do not reflect the views of the NHMRC. **Author contributions:** B.L.P. designed the experiments, performed cell culture, prepared and performed MS experiments, analyzed the data, and wrote the manuscript. G.Y. designed experiments, performed cell culture and molecular biology, prepared MS experiments, and wrote the manuscript. S.J.H. designed experiments, performed MS experiments, and wrote the manuscript. R.C. analyzed the data. X.M. performed cell culture and molecular biology. S.P. designed experiments and synthesized peptides. D.E.J. designed experiments, wrote the manuscript, and supervised the work. **Competing interests:** The authors declare that they have no competing interests. **Data and materials availability:** The targeted analysis results have been uploaded to the Panorama Repository for Targeted Proteomics (*36*) and are available through web viewing or direct download for analysis in Skyline (https://panoramaweb.org). The data are located within the "Metabolic Systems Biology—Usydney" Project in the "Phosphoproteomics of Insulin Signalling using DIA" folder. Access is available using the e-mail login: metabolicsystemsbiology@outlook.com and password: USydney1.

Submitted 17 November 2014
Accepted 5 May 2015
Final Publication 9 June 2015
10.1126/scisignal.aaa3139
Citation: B. L. Parker, G. Yang, S. J. Humphrey, R. Chaudhuri, X. Ma, S. Peterman, D. E. James, Targeted phosphoproteomics of insulin signaling using data-independent acquisition mass spectrometry. *Sci. Signal.* **8**, rs6 (2015).

Targeted phosphoproteomics of insulin signaling using data-independent acquisition mass spectrometry

Benjamin L. Parker, Guang Yang, Sean J. Humphrey, Rima Chaudhuri, Xiuquan Ma, Scott Peterman and David E. James (June 9, 2015)

Science Signaling **8** (380), rs6. [doi: 10.1126/scisignal.aaa3139]